ARCHIVE OF MECHANICAL ENGINEERING

DOI: 10.24425/ame.2025.157255 2025, Vol. 72, No. 4, pp. 647–670

Roman KRÓL [1]

Multibody dynamics model of the cycloidal gearbox with uniform discretization of the cycloidal wheel profile

Received 3 August 2025, **Revised** 4 November 2025, **Accepted** 7 November 2025, **Published online** 26 November 2025

Keywords: cycloidal gearbox, multibody dynamics, contact modelling, contact models, discretization, cycloidal gearbox model, motion equations integration, cycloidal gear train

This article presents the results obtained in the multibody dynamics model of the cycloidal gearbox with Hunt and Crossley contact modelling. The model is implemented in Fortran and uses the 2nd order Runge-Kutta method to integrate the motion equations. The contact modelling requires discretization of the cycloidal wheel profile. In previous models, the discretization has been performed using constant increments in the parameter of the cycloidal wheel equations. The presented version of the model uses uniform discretization of the cycloidal wheel, which is implemented using arc length calculation, bisection method and derivatives of the profile. The results show that the numerical solution of derivatives is the main issue in the model with uniform discretization. When the contact point lies near the inflection point of the cycloid, the radius of curvature tends to be infinite. The previous model, which used parameter discretization and calculated curvature based on the radius of a circle passing through three neighboring points on the cycloidal wheel, exhibited lower numerical errors and smoother time profiles of the dynamic variables. Despite the expectations that equal discretization would provide better energy stability, it turned out that the use of parametric discretization is simpler and more reliable.

1. Introduction

Cycloidal gearboxes are the mechanisms that combine the ability to work under heavy loads and have compact geometric dimensions. Contemporary research in this field includes fault diagnosis [1], dynamics [2, 3], stress analysis [4], kinematical and dynamical analysis [5, 6], kinematical error and contact analysis [7, 8], backlash [9, 10] and meshing modification [11]. Vibrations in these

✉ Roman KRÓL, email: r.krol@urad.edu.pl

[1] Casimir Pulaski Radom University, Radom, Poland

© 2025. The Author(s). This is an open-access article distributed under the terms of the Creative Commons Attribution (CC-BY 4.0, https://creativecommons.org/licenses/by/4.0/), which permits use, distribution, and reproduction in any medium, provided that the author and source are cited.

www.czasopisma.pan.pl PAN POLSKA AKADEMIA NAUK www.journals.pan.pl

mechanisms [3, 12–15] can be studied using sophisticated digital signal processing methods, and are one of the main side effects in the field of application of these devices. The angular velocity and torque at the output shaft are random signals modulated by the rolling contact phenomenon. Contemporary research in fault diagnosis methods employs various approaches to extracting signal features from the modulated output torque [15]. Despite the rich history of ideas in this discipline, the successful fault diagnosis is applied mainly to the cylindrical and planetary gearboxes [16–20]. Some of the contemporary works find that defects in the cycloidal wheel influence spectrum scattering [21]. Extraction of the features characterizing the cycloidal gearbox output torque is very complex, and research concerning this type of mechanism is not as popular as in the field of planetary gearboxes.

Significant vibration and noise make it difficult to apply cycloidal gearboxes in robotics applications, where motion should be precise. Further studies on the cycloidal gearbox dynamics allow one to find new designs and solutions, which can be successfully applied in industrial robots, winches, or electric bicycles. Modern dynamics studies analyze cycloidal gearboxes in compound mechanisms connected with planetary gearboxes [22–25]. Dynamical characteristics of these gearboxes' motion can be studied using engineering software (MSC Adams); however, interference through the scripting languages with Hertzian contact models is very laborious and often impossible. Commercial engineering software is, in many aspects, a black box, which is not exhaustively described in documentation and leaves the engineer with a small number of predefined options to choose from.

A good way to study cycloidal gearbox dynamics is using programmed models, which offer unlimited possibilities to apply new or modified contact models. The multibody dynamics method can be used to model the transient motion of the details of a multipart mechanism. In each iteration of the analysis, the contact modelling algorithm checks the interference between bodies and applies forces calculated with Hertzian theory in the force vector being a part of the multibody dynamics equations.

First attempts of programming multibody dynamics models showed that Matlab or Java are too slow for the analysis of the cycloidal gearbox working with the input speed of 500 RPM (8.33 Hz). The Fortran programming language has numerous facilities for operations on matrices and systems of equations. It is fast enough and very convenient for this type of application. First models [13, 26] were successfully implemented in Fortran. Visualization software has been programmed in Java with the OpenGL graphics library.

Several models [2, 3, 14, 27] introduce simplifications in the motion of cycloidal gearbox. These models can estimate dynamic quantities relevant to the gearbox and may be useful in the design process. However, it should be noted that in the cycloidal gearbox, the dynamic behavior at a given moment in time depends on previous states, particularly when random variations in depth of penetration occur between the external sleeves and the cycloidal wheel. In the model implemented in Fortran [26], which uses the multibody dynamics method, improper

www.czasopisma.pan.pl PAN POLSKA AKADEMIA NAUK www.journals.pan.pl

contact model can lead to energy accumulation, gradual rise in contact forces, oscillations and finally a non-convergent analysis. This proves that only properly configured Hertzian contact parameters (viscous damping, stiffness and force exponent) can simulate behavior of the cycloidal gearbox and this analysis should be transient with integration of the motion equations containing constraints and forces that change in each iteration of the analysis.

In this article, the model [26] (and its newer version with corrected contact stiffness solution [28]) has been improved by the application of the uniform discretization of the cycloidal wheel profile [29]. The parametric equations describing cycloidal wheel shape are given below and described in Table 1.

$$\begin{aligned} x(t) &= \frac{ez_k}{m}\cos(t) + e\cos(z_k t) - q\cos(t+\gamma), \\ y(t) &= \frac{ez_k}{m}\sin(t) + e\sin(z_k t) - q\sin(t+\gamma), \\ \gamma &= \operatorname{atan}\left[\frac{\sin(z_s t)}{\frac{1}{m} + \cos(z_s t)}\right]. \end{aligned} \tag{1}$$

Table 1. Parameters used in the equation (1)

Parameter	Description	Value
$x(t)$	Horizontal coordinate	–
$y(t)$	Vertical coordinate	–
t [rad]	Equation parameter	$0–2\pi$
e [m]	Eccentricity	0.0028
z_k	Number of external sleeves	16
z_s	Number of lobes	15
m	Short-width coefficient	0.7
q [m]	Radius of the external sleeve	0.006

Three models have been compared. In the first model, the discretization is based on constant increments in the parameter t of the equations (1). This leads to non-uniform distribution of the points in the cycloidal wheel profile. The second model contains uniform discretization, which is based on constant increments in the arc length of the cycloidal wheel. Two variants of discretization are shown in Fig. 1. The third model is designed in the MSC Adams software.

It is presented in Fig. 1 that in the uniform arc length discretization the distances between the successive points are equal, while in the parameter discretization, there are points concentrated in the regions of inflection, and the points are rare in the pits of the cycloidal wheel.

The uniform arc length discretization aims to obtain smooth time courses of the dynamic entities solved in the model. It was shown in [13] that the time courses

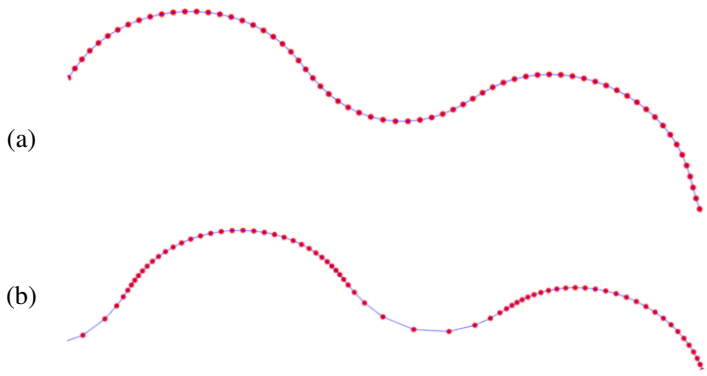

Fig. 1. Distribution of the contact points in the cycloidal wheel profile: (a) uniform arc length discretization and (b) parameter discretization. The presented discretization density is 600 points on the wheel profile

of the forces acting on the internal and external sleeves significantly depend on the number of points in the cycloidal wheel profile (the density of discretization).

2. Multibody dynamics model

The multibody dynamics model [29] has been implemented in GNU Fortran 95 and described in [13] and [15]. The system of equations (2) is solved in each iteration of the integration algorithm. Accelerations are integrated by the 2nd order Runge-Kutta method.

$$\begin{bmatrix} \mathbf{M} & -\mathbf{D}^T \\ \mathbf{D} & \mathbf{0} \end{bmatrix} \begin{bmatrix} \ddot{\mathbf{u}} \\ \boldsymbol{\lambda} \end{bmatrix} = \begin{bmatrix} \mathbf{F} \\ \boldsymbol{\gamma} \end{bmatrix}. \tag{2}$$

where: $\mathbf{M}$ – mass matrix (contains masses and moments of inertia of the parts), $\mathbf{D}$ – Jacobian matrix, $\mathbf{0}$ – zero matrix, $\ddot{\mathbf{u}}$ – solved accelerations, $\boldsymbol{\lambda}$ – solved reaction forces, $\mathbf{F}$ – vector of applied forces and moments, $\boldsymbol{\gamma}$ – right-hand side vector of the acceleration equations.

The model investigated in this article will be named *the model with uniform arc length discretization* [29], and the previous model [28] is *the model with parameter discretization*. The first one compared with [28] has many modifications. In the model with parameter discretization, contact stiffness was calculated based on the curvature at the given contact point. The curvature was calculated by solving for the radius of the circle that passes through the contact point and two neighboring points. In the model with the uniform arc length discretization, the radius of curvature

$$R = \frac{[x'(t_0)^2 + y'(t_0)^2]^{3/2}}{x'(t_0)y''(t_0) - y'(t_0)x''(t_0)} \tag{3}$$

www.czasopisma.pan.pl PAN POLSKA AKADEMIA NAUK www.journals.pan.pl

is solved based on the derivatives which have been solved using numerical interpolation:

$$x'(t) = \frac{x(t+h) - x(t-h)}{2h}, \tag{4}$$

$$y'(t) = \frac{y(t+h) - y(t-h)}{2h}, \tag{5}$$

$$x''(t) = \frac{x(t+h) - 2x(t) + x(t-h)}{h^2}, \tag{6}$$

$$y''(t) = \frac{y(t+h) - 2y(t) + y(t-h)}{h^2}. \tag{7}$$

The radius of curvature is used to calculate contact stiffness. This value should be bounded because, if the contact point occurs in the inflection region of the cycloid, the derivative will have a value close to zero, hence the value of the curvature radius will tend to infinity.

In the previous version of the software (the model with parameter discretization), which was described in [13], there were minor corrections introduced in stiffness calculation. This modification concerned an improper sign in the calculation of the distance between the center of the circle through the contact point and the center of the external sleeve. This distance is used to decide if the contact occurred in the concave or convex region of the cycloidal wheel.

There is a driver joint at the input shaft, which imposes an angular velocity of 500 RPM (8.33 Hz). The gearbox starts from a position of stillness and accelerates to full speed in 0.2 s. The analysis time is 0.5 s, and the time interval is constant, equal to 10^{-5} s. In models designed in MSC Adams and Fortran, the friction in the bearings and in the revolute joints was omitted.

3. Implementation of the uniform arc length discretization of the cycloidal wheel

Uniform arc length discretization was implemented in the Fortran module used before the integration of the motion equations. To find the progression of the parameter value in the cycloid equations (1) the equation for the arc length and the bisection method were used:

$$L = \int_a^b \sqrt{x'(t)^2 + y'(t)^2}\,\mathrm{d}t, \tag{8}$$

where: L – arc length, t – parameter of the cycloid equation, a – starting value of the parameter t, b – ending value of the parameter t, $x'(t)$, $y'(t)$ – first order derivatives of the parametric equations of the cycloid.

www.czasopisma.pan.pl PAN POLSKA AKADEMIA NAUK www.journals.pan.pl

The square root in equation (8) is integrated using the trapezoidal method. The bisection method is described in equations:

$$L = \int_0^{2\pi} \sqrt{x'(t)^2 + y'(t)^2}\,\mathrm{d}t, \tag{9}$$

$$L_0 = \frac{L}{N}, \tag{10}$$

$$f = \frac{a+b}{2}, \tag{11}$$

$$A = \int_t^a \sqrt{x'(t)^2 + y'(t)^2}\,\mathrm{d}t, \tag{12}$$

$$C = \int_t^f \sqrt{x'(t)^2 + y'(t)^2}\,\mathrm{d}t, \tag{13}$$

$$\begin{cases} (A - L_0) \cdot (C - L_0) < 0 \;\Rightarrow\; b = f, \\ (A - L_0) \cdot (C - L_0) \geq 0 \;\Rightarrow\; a = f \end{cases} \tag{14}$$

$$\frac{b-a}{2} < tol \;\Rightarrow\; t_{i+1} = \frac{a+b}{2}. \tag{15}$$

First, the length of the cycloid profile is determined (equation (9)) and divided by $N = 4000$ arcs in such a way that the elementary arc length is obtained using equation (10). The bisection method aims to find the parameter t, for which the arc length will be equal L_0. The central point of the interval (a, b) is found from equation (11). In this interval, the value of the t parameter will be sought. Then, the two arc lengths are determined: the arc length A (equation (12)) from the starting point to the beginning of the interval a, and the arc length C (equation (13)) from the starting point to the central point of the interval f. The two arc lengths, A and C, are compared with the elementary arc length L_0 (equation (14)). If the elementary arc length is between A and C, then the end of the interval becomes f. In the other case, the beginning of the interval becomes f. If half the difference between the boundary points of the interval is smaller than the tolerance value (tol), the parameter value t_{i+1} is determined as the average of the updated interval (a, b) (equation (15)).

The tolerance value has been set to 10^{-5}, and the results of the discretization have been checked by the visualization software (Fig. 1).

The results were also compared with the MSC Adams software. The model in this engineering software was designed using methods described in [3, 6, 12, 14]. The component bodies of the cycloidal gearbox are rigid, and these are mounted on the bearings, which simulate revolute joints. The bodies can rotate around the bearing mounting point.

www.czasopisma.pan.pl PAN POLSKA AKADEMIA NAUK www.journals.pan.pl

The 3D contact between the bodies in the MSC Adams model is achieved using triangulation of the surfaces. The Fortran models with uniform arc length discretization and those with parameter discretization are 2D. The contact modelling was configured using methods presented in [8, 30–32].

The MSC Adams model is shown in Fig. 2.

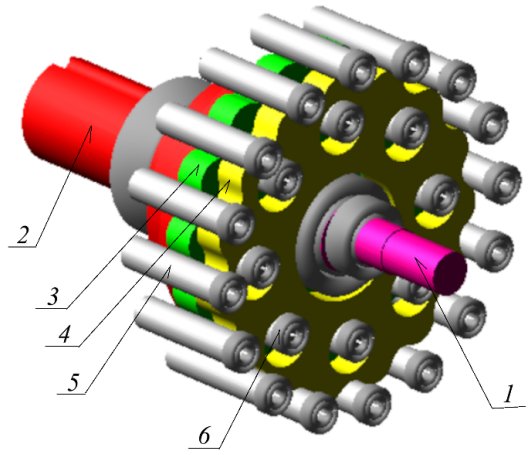

Fig. 2. MSC Adams model: 1 – input shaft, 2 – output shaft, 3 – internal cycloidal wheel, 4 – external cycloidal wheel, 5 – external sleeve, 6 – bearing between the internal pin and the internal sleeve

The triangulation mesh in the 3D contact in the MSC Adams is probably the cause for the higher contact times. The time courses from the MSC Adams model presented in the results chapter are wider than the time courses obtained in the Fortran model. This phenomenon was shown in [13]. The higher contact time intervals are caused by the lower values of backlash.

4. Contact parameters in the Fortran and MSC Adams models

The contact parameters in all models were intended to be equal (Table 2). Exceptionally, in the model with parameter discretization, the contact viscous damping was set to 200 Ns/m because of convergence issues. In the model with uniform parameter discretization and the MSC Adams, it was set to 300 Ns/m. The contact stiffness is also different in these models. It is due to the different methods of curvature solution, which are affected by the discretization. If the discretization is too dense, the solution of the curvature based on the circle passing through three neighboring points will be affected by the rounding errors and precision.

In Fortran models, the contact check is performed in each iteration of the motion equations integration algorithm. If the distance between the center of the

Table 2. Contact parameters in Fortran models and in MSC Adams

Entity	Fortran model with uniform arc length discretization [29]	Fortran model with parameter discretization [28]	MSC Adams model
Contact stiffness	Curvature dependent (Fig. 5), the radius of curvature could not be greater than 1 m	Curvature dependent (Fig. 6), the radius of curvature could not be greater than 1 m	31 622 777 N/m$^{1.5}$ (1000 N/mm$^{1.5}$) (constant stiffness)
Force exponent	1.5	1.5	1.5
Damping	300 Ns/m (Point contact)	200 Ns/m (Point contact)	300 Ns/m (3D contact)
Penetration depth, for which the contact is activated	0.0001 m	0.0001 m	0.0001 m
Static coefficient of friction	0.05 (increases from 0 to maximum value when the contact velocity (the velocity of deformation) reaches 0.00005 m/s)	0.05 (increases from 0 to maximum value when the contact velocity (the velocity of deformation) reaches 0.00005 m/s)	0.05
Dynamic coefficient of friction	0.05 (increases from 0 to maximum value when the contact velocity (the velocity of deformation) reaches 0.00005 m/s)	0.05 (increases from 0 to maximum value when the contact velocity (the velocity of deformation) reaches 0.00005 m/s)	0.05

sleeve and the point on the cycloidal wheel is smaller than the sleeve radius, then the contact normal force is calculated based on the following equation:

$$F_n = K\delta^p \pm Cv_n\,, \tag{16}$$

where: F_n – contact normal force, K – contact stiffness, δ – penetration, p – force exponent (the rate of penetration penalization), C – contact damping, v_n – contact normal velocity.

The masses and moments of inertia of the bodies being part of the models presented in this article are shown in Table 3.

Table 3. Masses and moments of inertia of the component bodies

Part name	Mass [kg]	Moment of inertia [kg m^2]
Input shaft	0.2341	$1.846 \cdot 10^{-6}$
Output shaft	1.6345	$1.373 \cdot 10^{-4}$
Cycloidal wheel	0.5998	$1.575 \cdot 10^{-4}$
External sleeve	0.048	$1.101 \cdot 10^{-5}$
Internal sleeve	0.048	$1.101 \cdot 10^{-5}$

www.czasopisma.pan.pl PAN POLSKA AKADEMIA NAUK www.journals.pan.pl

5. Circular approximation in the model with parameter discretization

In the model with parameter discretization, contact stiffness is determined based on the radius of curvature at the contact point. The radius of curvature is found using circular approximation of three neighboring points. After one point is detected as the contact point, two neighboring points are taken from the table containing points of the given cycloidal wheel. The center and the radius (equation (19) of the circle passing through these points are obtained from equation (18), which arise from (17) [33].

$$x^2 + y^2 + 2ax + 2by + c = 0, \tag{17}$$

$$\begin{bmatrix} 2x_1 & 2y_1 & 1 \\ 2x_2 & 2y_2 & 1 \\ 2x_3 & 2y_3 & 1 \end{bmatrix} \cdot \begin{bmatrix} a \\ b \\ c \end{bmatrix} = \begin{bmatrix} -\left(x_1^2 + y_1^2\right) \\ -\left(x_2^2 + y_2^2\right) \\ -\left(x_3^2 + y_3^2\right) \end{bmatrix}, \tag{18}$$

$$x_0 = -a, \quad y_0 = -b, \quad r = \sqrt{x_0^2 + y_0^2 - c}, \tag{19}$$

where: x_1, y_1, x_2, y_2, x_3, y_3 – coordinates of the first, second, and third point on the circle, x_0, y_0 – coordinates of the circle center point, r – circle radius, a, b, c – solved constants. The equations were solved using the Gauss elimination method implemented in Fortran.

6. Analysis results

Apart from the described models, where the derivative increment was set to 10^{-2}, additional analyses were run with a modification of the derivative increment, which affected the obtained value of the curvature radius.

The results of the performed analyses are the depth of penetration, the forces acting on the internal and external sleeves, the contact stiffness, the contact normal velocity and torque at the input and output shafts. When the contact appears, the cycloidal wheel is assumed to be rigid, and it penetrates the sleeve (loses its energy) according to the contact parameters.

The depth of penetration for the external sleeve is presented in Fig. 3, and for the internal sleeve in Fig. 4.

The contact modelling method uses contact stiffness and contact viscous damping (equation (16)). The contact stiffness depends on the radius of curvature, which is determined in different ways in the model with uniform arc length discretization and with parameter discretization. The depth of penetration was not compared to the MSC Adams results because, in this software, the contact is 3D, and it would be challenging to obtain maximum penetration depth based on the software functions.

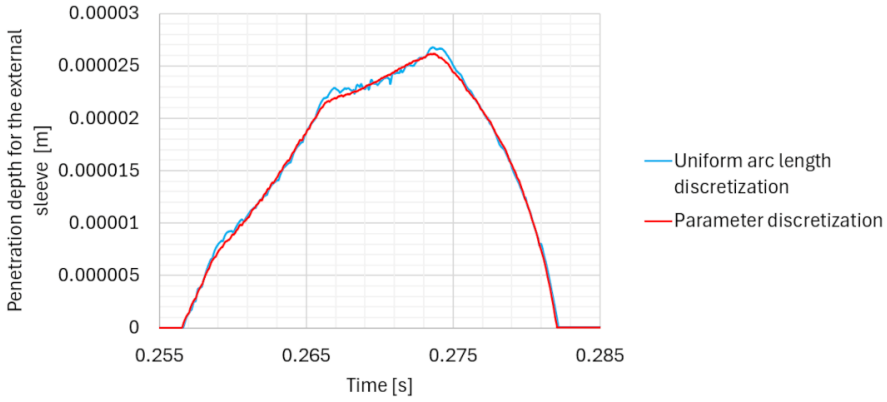

Fig. 3. Penetration depth for the external sleeve

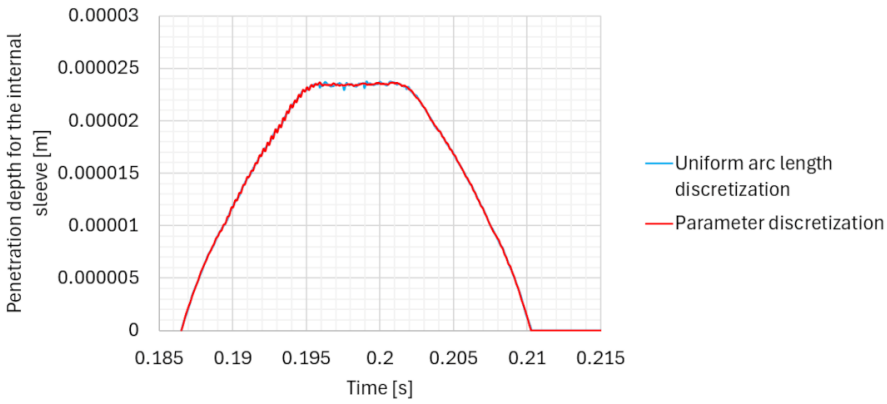

Fig. 4. Penetration depth for the internal sleeve

The time course of the penetration depth in the model with parameter discretization is smoother, and in the model with uniform arc length discretization there appear small amplitude oscillations, as shown in Fig. 3 for the contact with the external sleeve. The method of discretization has little to no effect when the contact with the internal sleeve occurs (Fig. 4). In both Fortran models, the constant curvature radius is used when calculating the contact stiffness for the internal sleeve and the cycloidal wheel.

The contact stiffness in the two Fortran models is shown in Figs. 5 and 6. In the model with uniform arc length discretization, the time course of contact stiffness is smooth, while in the model with parameter discretization it changes step by step in the region of the cycloidal wheel pit, where the discretization is rough (Fig. 1).

The time course of the force acting on one of the external sleeves is shown in Figs. 7 and 8. The results were compared to the MSC Adams simulation. The force obtained in MSC Adams has a longer acting time. As it was shown in [13], the

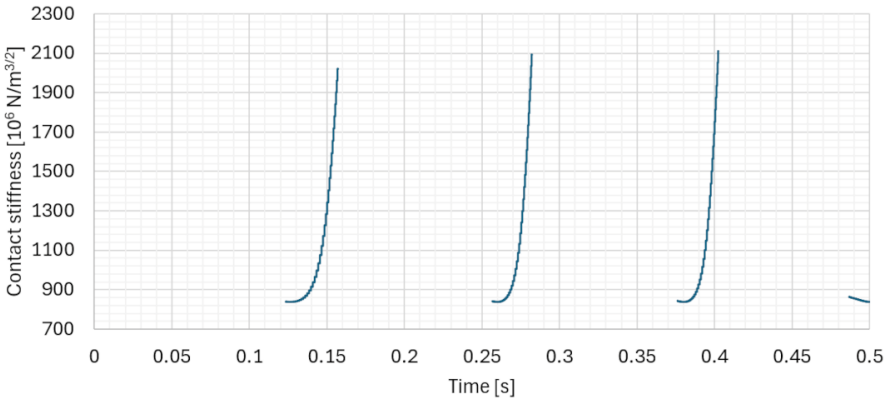

Fig. 5. Contact stiffness in the model with uniform arc length discretization

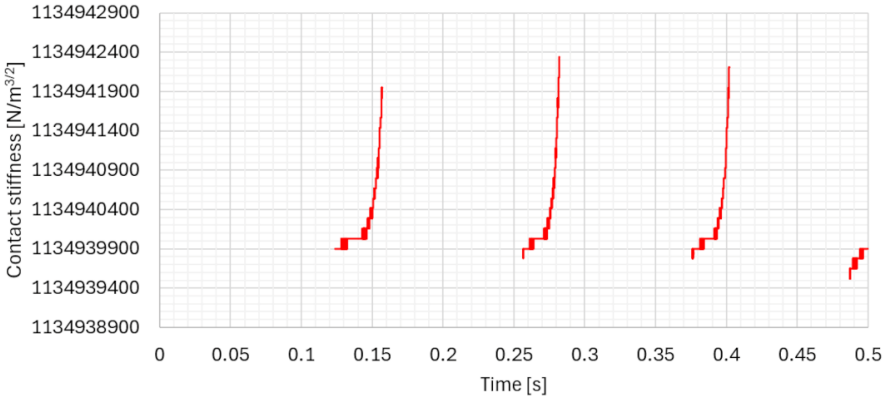

Fig. 6. Contact stiffness in the model with parameter discretization

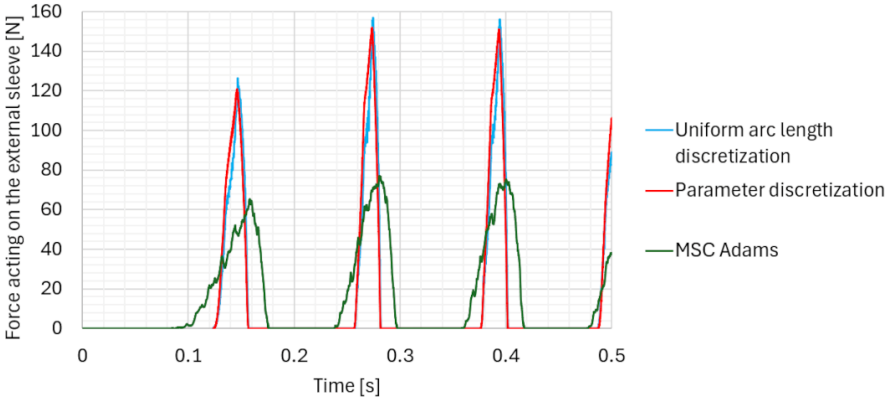

Fig. 7. Force acting on one of the external sleeves

acting time of the force depends on the backlash. Additional influence on this time course has contact modelling, which in MSC Adams is 3D and needs triangulation of the cycloidal wheel and external sleeve surfaces. The contact force is distributed over the nodes of the surface.

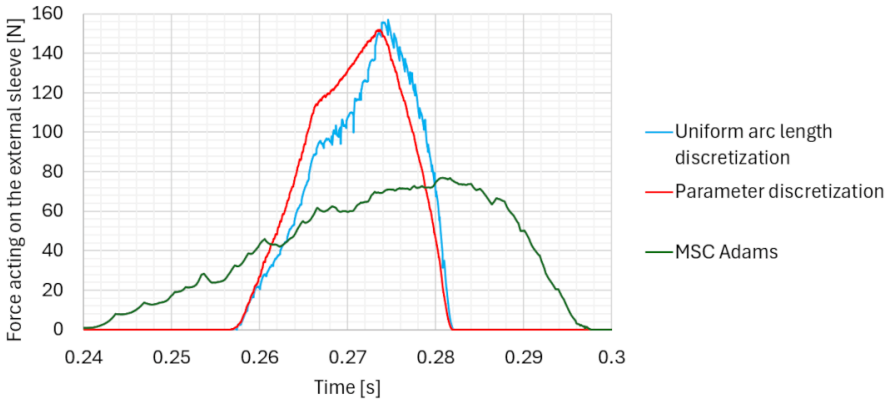

Fig. 8. Force acting on one of the external sleeves (enlarged detail)

The time course of the resulting force acting on one of the internal sleeves is presented in Figs. 9 and 10. Significant differences between the maximum values of the forces derived in Fortran models and MSC Adams arise from contact stiffness. There are small oscillations at the top of the force graph in the model with uniform arc length discretization.

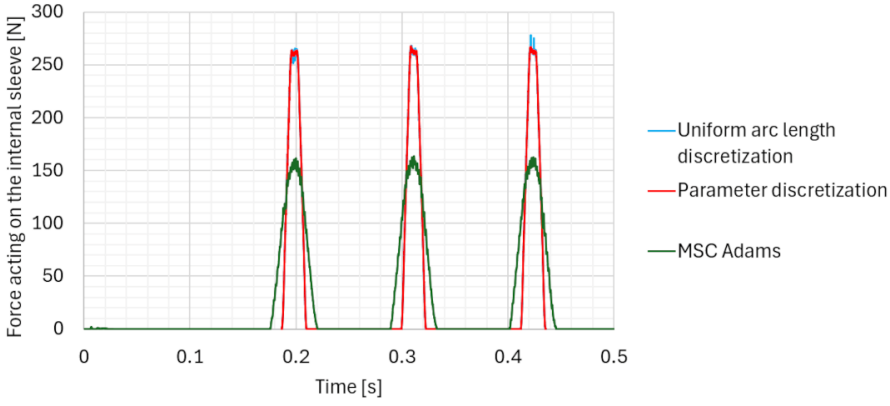

Fig. 9. Force acting on the internal sleeve

The small oscillations of the force acting on the external and internal sleeve can be caused by the numerical method of derivative calculation. These derivatives are used when determining the arc length in the discretization process and the

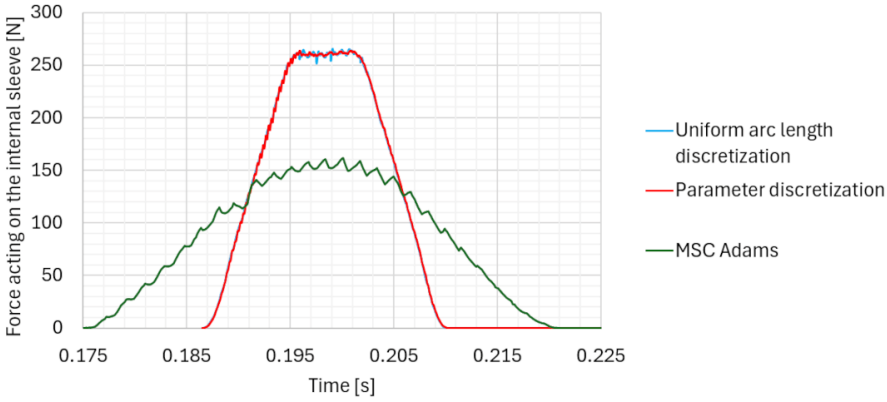

Fig. 10. Force acting on the internal sleeve (enlarged detail)

radius of curvature, which in this case has a greater significance. To investigate the influence of the numeric solution of the derivatives (equations (4)–(7)), additional analyses were performed. The derivative increment was set for various values from 10^{-4} to 1. The results of the force acting on the external sleeve in these analyses are presented in Fig. 11. It is shown that when the increment h of the derivative is too small, the value of derivative becomes unstable (the time course for $h = 10^{-4}$). When the h is too high, the precision of determining the derivative is low. When it is too small, there can be rounding errors, which can lead to $R \to \infty$. The value of R is bounded to 1 m. High values of R lead to unstable analysis, which is presented in Fig. 11.

The output shaft is loaded by a constant torque of 22 Nm. The geometry of the gearbox contains openings in the cycloidal wheels, where internal sleeves roll on their surface. The rolling motion is periodically accelerated and decelerated, hence the output torque oscillates, and it is additionally modulated by the contact.

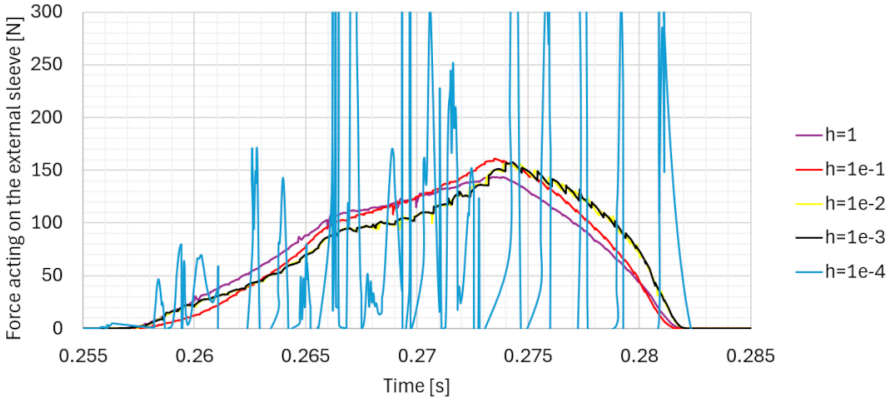

Fig. 11. Force acting on the external sleeve for various increments h (4)–(7) of the derivative used in arc length and radius of curvature (3) calculation

The output torque in Fortran models and in MSC Adams is shown in Figs. 12 and 13. In Fig. 12, impulses of significant amplitude emerge in the model with uniform arc length discretization. It is probably caused by inaccuracy of the numerical solution of the derivatives in the region near the inflection points of the cycloidal wheel. The impulses are bounded because the radius of curvature is limited to 1 m.

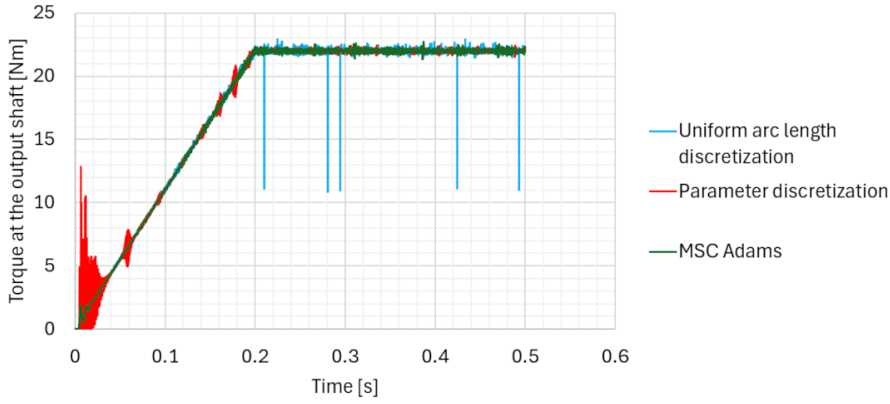

Fig. 12. Torque at the output shaft

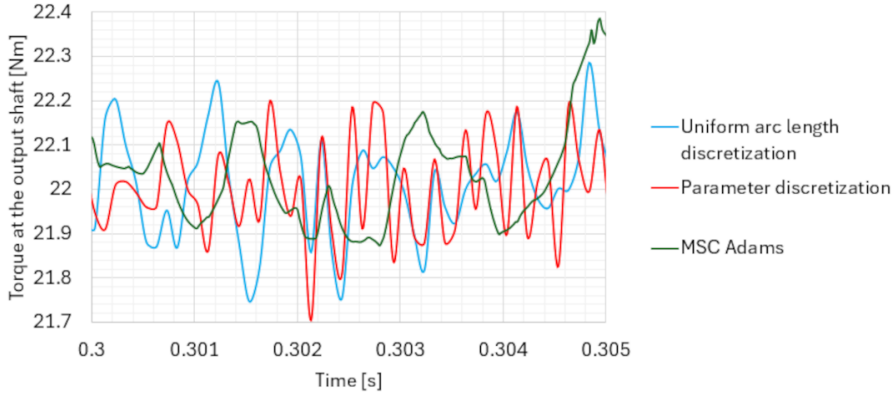

Fig. 13. Torque at the output shaft (enlarged detail from Fig. 12)

It is supposed that the model with uniform arc length discretization is less energetically stable than the model with parametric discretization. The peaks shown in Fig. 12 may disturb the energy balance of the model. For both models, elastic contact energy and dissipated energy were derived during the analysis from following equations:

$$U = \frac{K}{1.5+1}\delta^{1.5+1}, \tag{20}$$

www.czasopisma.pan.pl PAN POLSKA AKADEMIA NAUK www.journals.pan.pl

$$P_{di} = Cv_n^2, \tag{21}$$

$$D_{n+1} = D_n + 0.5(P_{di,n+1} + P_{di,n})\Delta t, \tag{22}$$

where: U – elastic contact energy, K – contact stiffness, δ – contact penetration between one of the cycloidal wheels and one of 16 external sleeves, 1.5 – force exponent (see equation (16)), P_{di} – dissipated power, C – contact viscous damping, v_n – contact normal velocity (relative velocity of the two contact points, one in the cycloidal wheel and one in the external sleeve), D – dissipated energy, n – iteration number in the 2nd order Runge-Kutta method, Δt – constant time increment in the analysis.

In Figs. 14 and 15, the contact elastic energy is shown for the model with uniform arc length discretization and for the model with parametric discretization, respectively. In Fig. 14, the contact elastic energy for the consecutive external

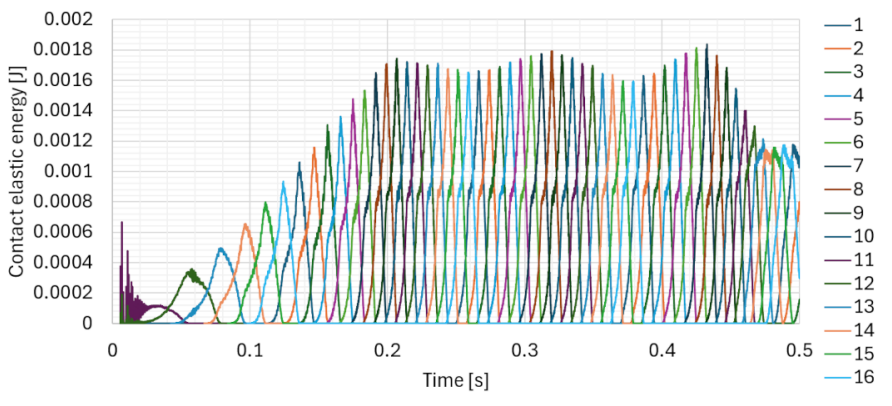

Fig. 14. Contact elastic energy in the model with uniform arc length discretization for the 1–16 external sleeves and external cycloidal wheel

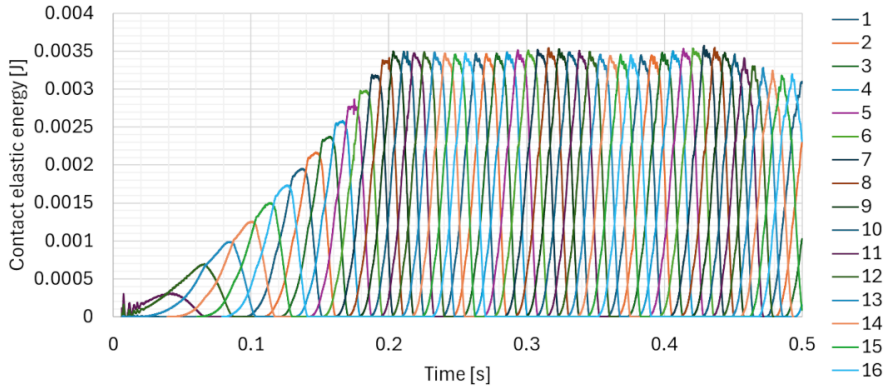

Fig. 15. Contact elastic energy in the model with parameter discretization for 1–16 external sleeves and external cycloidal wheel

sleeves is significantly modulated. Finally, at 0.45 s, there is an increase in the energy oscillation amplitude, and the model starts to oscillate and becomes non-convergent. The highest obtained analysis time with convergent results was nearly 0.65 s in both models. In future versions of the model, attempts to apply a more accurate Runge-Kutta method will be made. Unfortunately, it can lead to significantly greater analysis time.

In Figs. 16 and 17, the dissipated energy is shown for the same models. In the period of first 0–0.1 s of analysis, there appear high oscillations of contact normal velocity. The maximum dissipation energy oscillations in this period are 0.00094 J for the model with uniform arc length discretization and 0.000559 J for the model with parametric discretization. Fig. 16 shows that in the model with uniform arc length discretization, the changes of the dissipated energy are less regular than in the model with parameter discretization (Fig. 17).

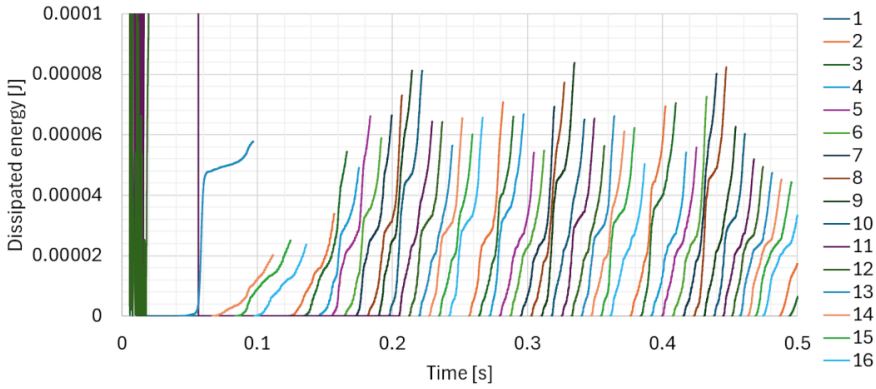

Fig. 16. Dissipated energy in contact between 1–16 external sleeves and the external cycloidal wheel (uniform arc length discretization)

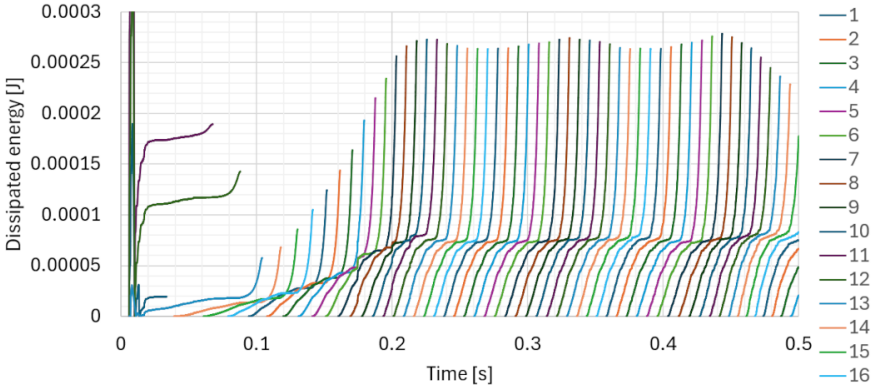

Fig. 17. Dissipated energy in contact between 1–16 external sleeves and the external cycloidal wheel (parameter discretization)

The torque at the input shaft was found based on the forces acting at the eccentric cams of the input shaft, on which the cycloidal wheels are mounted. Contact modelling in MSC Adams is 3D, and it causes higher losses than contact modelling in Fortran models. Figs. 18 and 19 show that contact modelling and discretization have a significant influence on the efficiency of the model. The viscous damping component of the contact significantly influences energy losses in the numerical model. For example, in the MSC Adams analysis performed for 10000 Ns/m the average value of the input torque was −1.8 Nm.

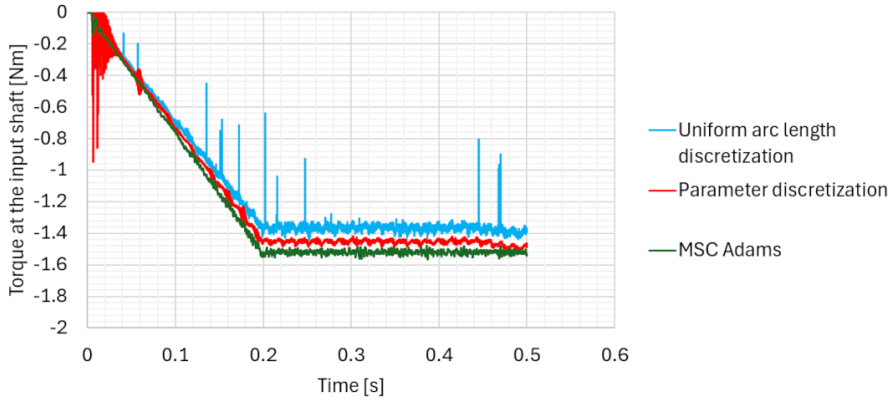

Fig. 18. Torque at the input shaft

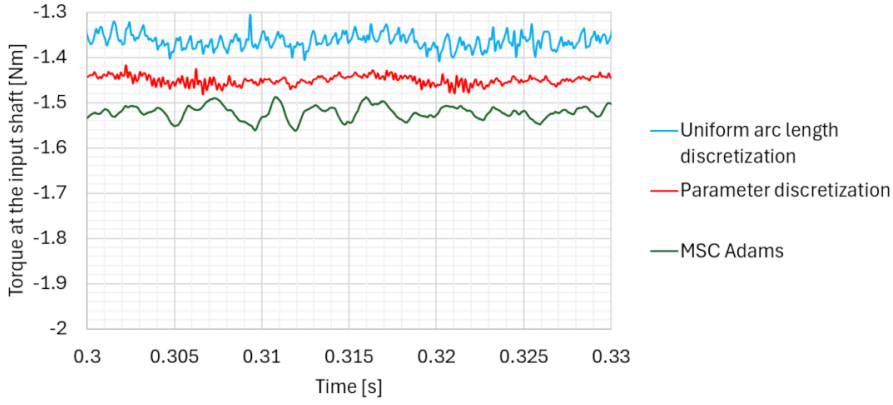

Fig. 19. Torque at the input shaft (enlarged detail)

The torque at the output shaft was determined in the model with uniform arc length discretization for various derivative increments. The results are shown in Fig. 20. Different graphs for each derivative increment prove that the instantaneous values of the output torque have different values, dependent on the previous cycles of analysis. The output torque is a random signal. Each contact interaction has different

energy characteristics. A significant issue in programming multibody models of cycloidal gearboxes is the setup of the contact parameters. The values of these parameters should be relevant to the specified model to avoid energy imbalance in the numerical model. The unbalanced model will lead to non-convergence.

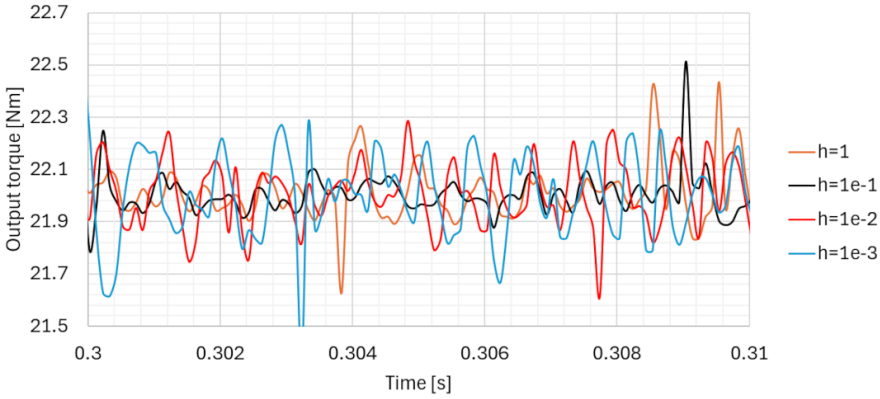

Fig. 20. Torque at the output shaft in the model with uniform arc length discretization for various increments of the derivatives

In contrast to the engineering software, programming models of the cycloidal gearbox allow analysis of the contact characteristics. One of them is the relative velocity of the points being in contact. In Fortran models, in each iteration of the Runge-Kutta algorithm, each point of the cycloidal wheel is checked for interference with the internal or external sleeve. If the point of the cycloidal wheel is in contact, the normal vector is found, and in the direction of the normal vector, the point on the sleeve is determined. Based on the relative velocity of these two points, the contact normal force is calculated using equation (16). The relative velocity of contact points (one in the cycloidal wheel and one in the external sleeve) is shown in Figs. 21 and 22. This quantity is equivalent to the speed of deformation of the sleeve. It depends on the contact stiffness, contact viscous damping and the kinematics of the cycloidal wheel. External sleeves are mounted in the housing, and they do not move. In the case of the internal sleeve, the velocity of the sleeve is significant. The relative velocity of contact points has a positive sign when the points move apart from each other and a negative sign when the contact force causes unloading and motion towards the opposite direction. During unloading, the damping component of the force is subtracted from the overall value of the contact force, as presented in equation (16). The subtracted part is responsible for the contact energy losses.

In Figs. 23 and 24, the relative velocity of the contact points (one in the cycloidal wheel and one in the internal sleeve) is presented. In enlarged Figs. 22 and 24, the peaks in the model with uniform arc length discretization are visible. They are caused by the numerical computation of the derivatives, which influence

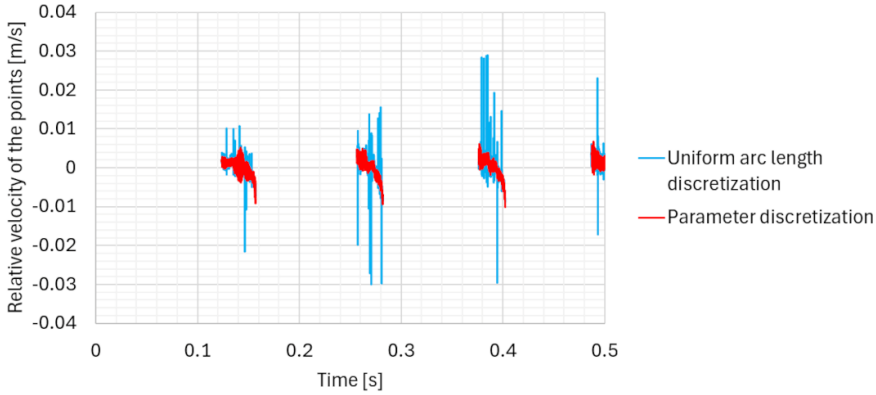

Fig. 21. Relative velocity of the contact points: one on the cycloidal wheel and one on the external sleeve

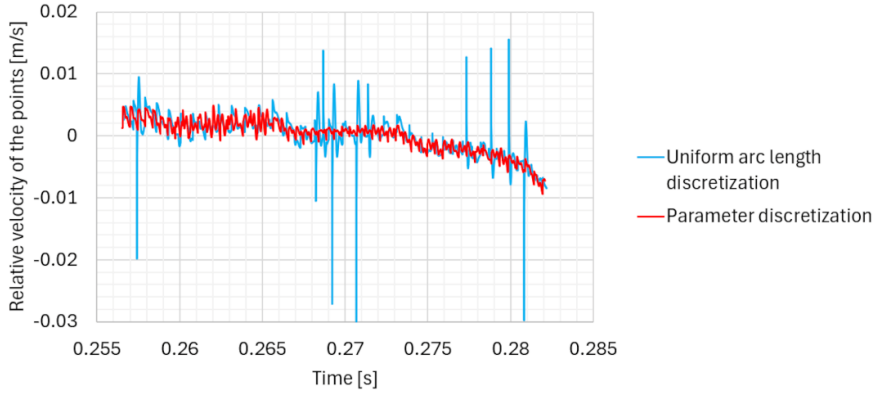

Fig. 22. Relative velocity of the contact points: one on the cycloidal wheel and one on the external sleeve (enlarged detail)

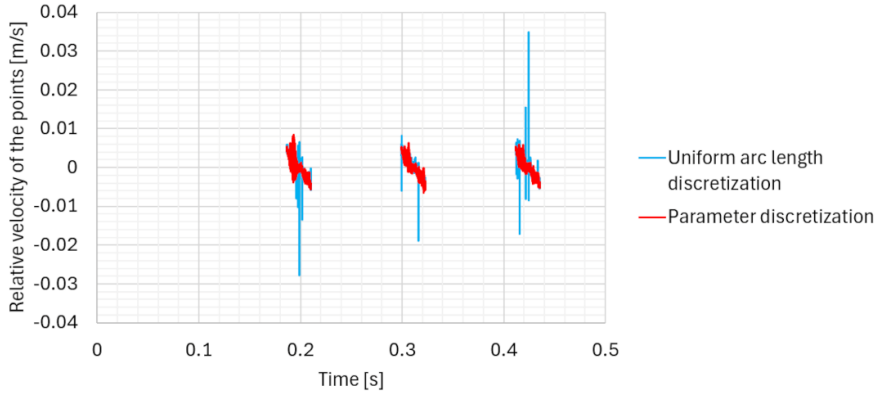

Fig. 23. Relative velocity of the contact points: one on the cycloidal wheel and one on the internal sleeve

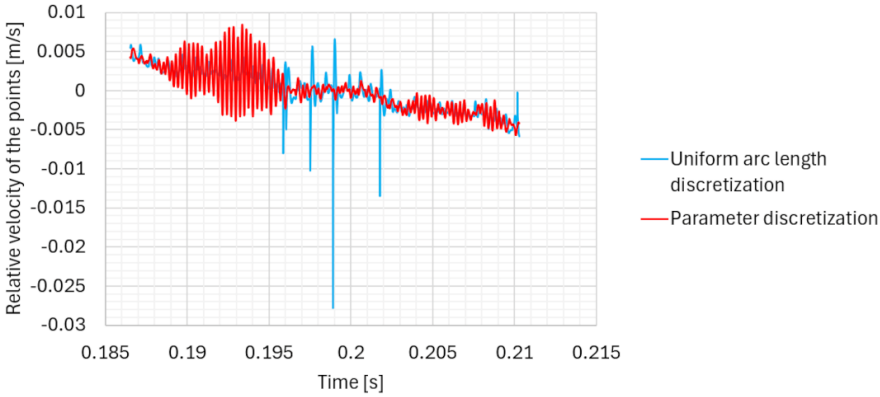

Fig. 24. Relative velocity of the contact points: one on the cycloidal wheel and one on the internal sleeve (enlarged detail)

the radius of curvature. However, in Fig. 24, it is shown that the model with parameter discretization has significantly higher oscillations than the model with uniform arc length discretization. It is worth noting that discretization was designed for the cycloidal wheel profile and not for the openings in the cycloidal wheel, where internal sleeves are placed.

7. Discussion of results

According to [13], the application of the finer discretization should lead to the smooth time courses of the dynamical quantities obtained from the multibody dynamics model. This research shows that better discretization can improve the solution of the relative velocity of the contact points (Figs. 21–24). Unfortunately, peaks arise in the time courses of other quantities (torques at the input and output shafts), which results from errors in determining the curvature radius near the inflection points. The amplitude of these peaks can be curbed by applying limits on the curvature radius. The main disadvantage of this discretization method is that local, high values of curvature radius influence contact stiffness which is an important component of the energy balance in the iterative simulation process.

The analysis of the energy balance (Figs. 14–17) shows that the model with parameter discretization is more stable than the model with uniform arc length discretization. In the graph of contact elastic energy, one can see that the oscillations during the contact with the successive external sleeves have significantly lower amplitude in the model with parameter discretization than those in the uniform discretization model. The same is true for dissipated energy, which is significantly disturbed in this case, as seen in Fig. 16. Peak values of the dissipated energy for the uniform discretization model are also less regular than for the parameter discretization model.

www.czasopisma.pan.pl PAN POLSKA AKADEMIA NAUK www.journals.pan.pl

If the model uses parameter discretization and the discretization is fine enough, with a high number of points on the cycloidal wheel profile, the analysis can be convergent for longer, and the issue of energy balance is less significant. Too dense discretization can lead to the problems with computation of the curvature radius. In this case, the derivatives of the profile should be used despite all the drawbacks of this method.

The contact viscous damping is the source of efficiency decrease in the gearbox, as it influences the value of the torque at the input shaft (Figs. 18 and 19). Convergence of the analysis significantly depend on this contact parameter.

Time courses of the forces acting on the external and internal sleeves are wider in the MSC Adams model than in Fortran models. When 3D contact modelling is used with triangulation of the surfaces, the backlash parameters can be different in both models.

Peak-to-peak values of the torque at the output shaft (Fig. 13) are similar in all models. In the Fortran models, there are increased oscillations in the first iterations of analysis, which are caused by the stabilization of the numerical process due to the first occurrences of point-to-point contact. Solving output torque in Fortran models for various derivative increments (Fig. 20) showed that the time courses of these variables are completely different. The oscillations of the output torque have similar amplitudes. However, the oscillations are differently modulated by the contact phenomenon, and their graphs are shifted in time. It proves that the output torque in the cycloidal gearbox is a random signal which depends on the previous contact interactions between the cycloidal wheels and sleeves.

Fig. 11 shows the time courses of the force acting on the external sleeve determined for various derivative increments. The time courses for the highest increments are smooth, while small oscillations occur for the low values of the derivative increment, which could be related to the precision of the derivative.

Determining the curvature radius based on the circle passing through three neighboring points results in smoother time courses of the force acting on the external sleeve. This confirms that the solution based on parameter discretization is a better choice, as it is more stable and predictable regarding energy balance.

Figs. 22 and 24 show peaks in the time courses of the relative velocity of the contact points. The same phenomenon occurs for the external and internal sleeves. The application of parameter discretization can cause local oscillations. However, high amplitude peaks do not disturb the numerical process, contrary to the case of the uniform arc length discretization.

8. Conclusions

The analyzes performed in the Fortran models with uniform arc length discretization and parameter discretization showed that the application of the uniform distribution of the points in the cycloidal wheel profile does not lead to better configuration of the model.

www.czasopisma.pan.pl PAN POLSKA AKADEMIA NAUK www.journals.pan.pl

The application of uniform arc length discretization showed that the solution of the curvature radius based on the circle passing through the three neighboring points leads to numerical problems. Therefore, the method of derivatives was applied. It becomes difficult to guarantee a smooth time course of the curvature radius when the discretization is dense and the solution uses a circular approximation of the curvature radius. The parametric discretization model is non-convergent for dense discretization. Using uniform arc length discretization requires solving the curvature radius based on the first- and second-order derivatives of the cycloidal wheel profile and bounding this quantity in the regions of inflection points. The main drawbacks of this solution are significant peaks in the time courses of the torques and relative velocities of contact points, which can disturb the energy balance of the numerical solution. Despite expectations related with uniform discretization, the parametric discretization model turned out to be simpler and showed better energy balance than the uniform discretization model. This solution is better when the number of discretization points is not too high, otherwise errors may appear in the curvature solution. The best solution for the point-to-point contact is probably the application of variable density discretization, which will be investigated in further research.

Acknowledgements

This research utilized the MSC Software National Scientific Software License, operated by the TASK Computer Centre in Gdańsk (Poland). This license was funded by a computational grant obtained by Casimir Pulaski Radom University in Poland.

References

[1] I. Komorska, K. Olejarczyk, A. Puchalski, M. Wikło, and Z. Wołczyński. Fault diagnosing of cycloidal gear reducer using statistical features of vibration signal and multifractal spectra. *Sensors*, 23(3):1645, 2023. doi: 10.3390/s23031645.

[2] M. Blagojević, M. Matejić, and N. Kostić. Dynamic behaviour of a two-stage cycloidal speed reducer of a new design concept. *Tehnicki Vjesnik*, 25:291–298, 2018. doi: 10.17559/TV-20160530144431.

[3] M. Wikło, R. Król, K. Olejarczyk, and K. Kołodziejczyk. Output torque ripple for a cycloidal gear train. *Proceedings of the Institution of Mechanical Engineers, Part C: Journal of Mechanical Engineering Science*, 233(21-22):7270–7281, 2019. doi: 10.1177/0954406219841656.

[4] N. Kumar, V. Kosse, and A. Oloyede. A new method to estimate effective elastic torsional compliance of single-stage Cycloidal drives. *Mechanism and Machine Theory*, 105:185–198, 2016. doi: 10.1016/j.mechmachtheory.2016.06.023.

[5] C.F. Hsieh. The effect on dynamics of using a new transmission design for eccentric speed reducers. *Mechanism and Machine Theory*, 80:1–16, 2014. doi: 10.1016/j.mechmachtheory.2014.04.020.

[6] R. Król. Kinematics and dynamics of the two stage cycloidal gearbox. *AUTOBUSY – Technika, Eksploatacja, Systemy Transportowe*, 19(6):523–527, 2018. doi: 10.24136/atest.2018.125.

www.czasopisma.pan.pl PAN POLSKA AKADEMIA NAUK www.journals.pan.pl

[7] K.S. Lin, K.Y. Chan, and J.J. Lee. Kinematic error analysis and tolerance allocation of cycloidal gear reducers. *Mechanism and Machine Theory*, 124:73–91, 2018. doi: 10.1016/j.mechmachtheory.2017.12.028.

[8] L.X. Xu, B.K. Chen, and C.Y. Li. Dynamic modelling and contact analysis of bearing-cycloid-pinwheel transmission mechanisms used in joint rotate vector reducers. *Mechanism and Machine Theory*, 137:432–458, 2019. doi: 10.1016/j.mechmachtheory.2019.03.035.

[9] D.C.H. Yang and J.G. Blanche. Design and application guidelines for cycloid drives with machining tolerances. *Mechanism and Machine Theory*, 25(5):487–501, 1990. doi: 10.1016/0094-114X(90)90064-Q.

[10] J.W. Sensinger. Unified approach to cycloid drive profile, stress, and efficiency optimization. *Journal of Mechanical Design*, 132(2):024503, 2010. doi: 10.1115/1.4000832.

[11] Z.Y. Ren, S.M. Mao, W.C. Guo, and Z. Guo. Tooth modification and dynamic performance of the cycloidal drive. *Mechanical Systems and Signal Processing*, 85:857–866, 2017. doi: 10.1016/j.ymssp.2016.09.029.

[12] R. Król. Analysis of the backlash in the single stage cycloidal gearbox. *Archive of Mechanical Engineering*, 69(4):693–711, 2022. doi: 10.24425/ame.2022.141521.

[13] R. Król and K. Król. Multibody dynamics model of the cycloidal gearbox, implemented in Fortran for analysis of dynamic parameters influenced by the backlash as a design tolerance. *Acta Mechanica et Automatica*, 17(2):272–280, 2023. doi: 10.2478/ama-2023-0031.

[14] R. Król. Resonance phenomenon in the single stage cycloidal gearbox. Analysis of vibrations at the output shaft as a function of the external sleeves stiffness. *Archive of Mechanical Engineering*, 68(3):303–320, 2021. doi: 10.24425/ame.2021.137050.

[15] R. Król. Analysis of the single stage cycloidal gearbox with lobe defects. Fault diagnosis attempts using coherence function and Morris minimum-bandwidth wavelets. *Archive of Mechanical Engineering*, 70(3):409–431, 2023. doi: 10.24425/ame.2023.146846.

[16] Y. Lei, D. Han, J. Lin, and Z. He. Planetary gearbox fault diagnosis using an adaptive stochastic resonance method. *Mechanical Systems and Signal Processing*, 38(1):113–124, 2013. doi: 10.1016/j.ymssp.2012.06.021.

[17] G. D'Elia, E. Mucchi, and M. Cocconcelli. On the identification of the angular position of gears for the diagnostics of planetary gearboxes. *Mechanical Systems and Signal Processing*, 83:305–320, 2017. doi: 10.1016/j.ymssp.2016.06.016.

[18] X. Chen and Z. Feng. Time-frequency space vector modulus analysis of motor current for planetary gearbox fault diagnosis under variable speed conditions. *Mechanical Systems and Signal Processing*, 121:636–654, 2019. doi: 10.1016/j.ymssp.2018.11.049.

[19] C. Wang, H. Li, J. Ou, R. Hu, S. Hu, and A. Liu. Identification of planetary gearbox weak compound fault based on parallel dual-parameter optimized resonance sparse decomposition and improved MOMEDA. *Measurement*, 165:108079, 2020. doi: 10.1016/j.measurement.2020.108079.

[20] W. Teng, X. Ding, H. Cheng, C. Han, Y. Liu, and H. Mu. Compound faults diagnosis and analysis for a wind turbine gearbox via a novel vibration model and empirical wavelet transform. *Renewable Energy*, 136:393–402, 2019. doi: 10.1016/j.renene.2018.12.094.

[21] Y. E, Z. Liu, H. Chen, Y. Zhang, Z. Li, H. Feng, and Z. Feng. Dynamic modeling and vibration analysis for fault diagnosis of rotate vector reducers. *Mechanical Systems and Signal Processing*, 224:111965, 2025. doi: https://doi.org/10.1016/j.ymssp.2024.111965.

[22] Y. Qiao, H. Wang, J. Cao, and Y. Lei. Sound-vibration spectrogram fusion method for diagnosis of RV reducers in industrial robots. *Mechanical Systems and Signal Processing*, 214:111411, 2024. doi: https://doi.org/10.1016/j.ymssp.2024.111411.

[23] D. Guo, Y. Zhang, X. Chen, H. Peng, Z. Jiang, H. Ma, and W. Du. Data-driven fault identification method of RV reducer used in industrial robot. *Heliyon*, 10(22):e40115, 2024. doi: 10.1016/j.heliyon.2024.e40115.

[24] T.G. Kormin and J-D.B. Tsumbu. Cycloidal reducer with rotation external ring gear. *IOP Conference Series: Materials Science and Engineering*, 971:042072, 2020. doi: 10.1088/1757-899X/971/4/042072.

[25] C. Klas and T. Asfour. Reaching torque-velocity profiles of human muscles: the adaptive cycloidal linear drive. *IEEE/ASME Transactions on Mechatronics*, 28(6):3470–3479, 2023. doi: 10.1109/TMECH.2023.3268556.2023.

[26] R. Król. Software for the cycloidal gearbox multibody dynamics analysis, implemented in Fortran. (Purpose: presentation of the results in the scientific article). Zenodo, Mar. 2023, doi: 10.5281/ZENODO.7729842.

[27] R. Król, M. Wikło, K. Olejarczyk, K. Kołodziejczyk, and A. Zieja. Optimization of the one stage cycloidal gearbox as a non-linear least squares problem. In T. Uhl (ed.): *Advances in Mechanism and Machine Science. IFToMM WC 2019*, pages 1039–1048, Springer, Cham, 2019. doi: 10.1007/978-3-030-20131-9_103.

[28] R. Król. Multibody dynamics model of the cycloidal gearbox (Fortran implementation). Zenodo, Oct. 2025. doi: 10.5281/zenodo.17362553.

[29] R. Król. Multibody dynamics model of the cycloidal gearbox with equal discretization of the cycloidal discs (Fortran sources). Zenodo, Oct. 2025. doi: 10.5281/zenodo.17359732.

[30] MSC Software, MSC Adams Solver Documentation.

[31] MSC Software, MSC Adams View Documentation.

[32] P. Flores and H.M. Lankarani. *Contact Force Models for Multibody Dynamics*. Springer International Publishing, Cham, 2016. doi: 10.1007/978-3-319-30897-5.

[33] Timur and Anton. Equation of a circle passing through 3 given points. planetcalc.com, 2018.